Journal Pre-proof

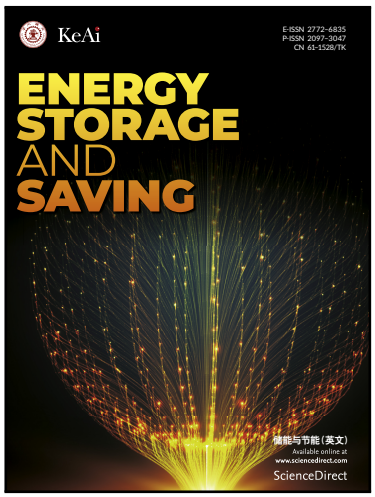

Passive battery thermal management and thermal safety protection based on hydrated salt composite phase change materials

Jingshu Zhang , Qian Liu , Xiaole Yao , Chen Sun , Xiaoqing Zhu , Chao Xu , Xing Ju

PII: S2772-6835(24)00037-2
DOI: https://doi.org/10.1016/j.enss.2024.08.003
Reference: ENSS 82

To appear in: *Energy Storage and Saving*

Received date: 20 March 2024
Revised date: 21 June 2024
Accepted date: 23 August 2024

Please cite this article as: Jingshu Zhang , Qian Liu , Xiaole Yao , Chen Sun , Xiaoqing Zhu , Chao Xu , Xing Ju , Passive battery thermal management and thermal safety protection based on hydrated salt composite phase change materials, *Energy Storage and Saving* (2024), doi: https://doi.org/10.1016/j.enss.2024.08.003

Passive battery thermal management and thermal safety protection based on hydrated salt composite phase change materials

Authors:

Jingshu Zhang[a], Qian Liu[a], Xiaole Yao[a], Chen Sun[a], Xiaoqing Zhu[a], Chao Xu[a], Xing Ju[a]*

[a]Key Laboratory of Power Station Energy Transfer Conversion and System of MOE, North China Electric Power University, Beijing 102206, PR China

Corresponding author:

Xing Ju

*Corresponding author. Tel.: +86 10 61773876.

E-mail addresses: scottju@ncepu.edu.cn

Abstract

Lithium-ion batteries (LIBs) are progressing towards higher energy densities, extended lifespans, and improved safety. However, battery thermal management systems are facing increased demand owing to high-rate charging and discharging, dynamic operating conditions, and heightened thermal safety concerns. Therefore, this paper proposes a novel composite phase change material (CPCM) comprising Na_2SO_4-$10H_2O$ as the core phase change material (PCM) and expanded graphite as the thermal conductivity enhancer. The CPCM offers high latent heat, superior thermal conductivity, and a two-stage temperature control function for battery thermal management and

safety. The optimal mass CPCM ratio, determined through comprehensive characterization and thermal property tests, resulted in a melting point of 29.05 °C, latent heat of 183.7 $J \cdot g^{-1}$, and high thermal conductivity of 3.926 $W \cdot m^{-1} \cdot K^{-1}$. During normal LIB operations, the CPCM efficiently absorbs and transfers heat, reducing the peak LIB temperature from 66 to 34 °C at 15 °C ambient temperature during a 3.7C high-rate discharge. Under dynamic conditions, the peak temperatures across the three cycles were consistently controlled at 36.7, 36.4, and 35.8 °C, respectively. In a thermal runaway state, the thermochemical heat storage of hydrated salt dehydration effectively slowed LIB temperature increase, delaying the time to reach 130 °C by 187 s. Suppression of the temperature rise outside the CPCM, combined with an extended dehydration plateau of up to 320 s, prevented the occurrence and propagation of thermal runaway in the battery.

Keywords: Battery thermal management system, Thermal runaway, Lithium-ion battery, Composite phase change materials, Hydrated salt, Dehydration

1.Introduction

In response to urgent global warming and environmental pollution challenges, many nations have pledged to curtail carbon emissions and achieve carbon neutrality by the middle of the century [1]. Electric vehicles (EVs) and battery energy storage systems have garnered significant attention as critical solutions for alleviating environmental stress and addressing the growing scarcity of natural resources [2]. Ensuring the optimal and efficient performance of power or energy storage batteries underscores the increasing significance of research in battery-related domains. Lithium-ion batteries (LIBs) have been widely used in power-driven and energy-storage systems [3] due to their high energy/power density, extended cycle life, minimal self-discharge rate, high stability, and safety features [1,4,5]. However, LIBs exhibit high temperature sensitivity, with high or low temperatures compromising their performance and lifespan [6]. The acceptable operating temperature range of LIBs is −20 to 60 °C [7], with an optimal range of 20 to 40 °C [8]. Thus, a well-designed and efficient battery thermal management system (BTMS) is necessary under the normal operating conditions of an LIB [9]. During daily usage, LIBs may experience abuse, such as overcharge/overdischarge, short circuiting, or exposure to high external temperatures, which can increase the internal battery temperature [10]. If not correctly dissipated to the surroundings, this temperature increase can trigger self-induced thermal runaway (TR), resulting in catastrophic damage [11]. The importance of a thermal safety protection system to mitigate the risk of TR in LIBs should not be overstated. For the future development of BTMS, a possible goal is to provide

comprehensive solutions that address the thermal management challenges and potential risks associated with TR.

BTMS are commonly classified into active [12–14] and passive thermal management systems [15–18] and are further categorized by diverse cooling methods, such as air, liquid, phase change materials, heat pipes, and hybrid systems [19]. Active BTMS are commonly used but have limitations such as disturbed reliability when dealing with extreme conditions, especially TR. Furthermore, it requires additional equipment and its cost and complexity are significantly increased [20].

Phase change material (PCM) is used for standard passive thermal management as it absorbs heat from batteries during phase changes, maintaining their working temperature within an appropriate range without an additional energy supply [21]. However, traditional organic PCMs, which have been extensively explored and applied in BTMS, have limited temperature control capabilities and struggle to manage the thermal behavior of batteries effectively over a broad temperature range. The latent heat densities of the PCMs (~150 $kJ \cdot kg^{-1}$) are insufficient for storing the significant heat released (~880 $kJ \cdot kg^{-1}$) during battery TR [22]. Upon the depletion of the latent heat, the increased thermal conductivity of the PCMs can accelerate the propagation of TR [23]. Additionally, the flammability of organic PCMs poses the risk of combustion and explosion, mainly when TR is triggered [24]. Consequently, the concurrent advancement of technologies applicable to BTMS and the mitigation of TR are paramount for enhancing the safety of LIB systems [2].

As inorganic PCMs, hydrated salt materials possess excellent features, including high latent heat storage density, flame retardancy, and commercial availability at low cost [25]. As a thermochemical heat storage material, it has advantages such as high heat storage density, small heat storage volume, minimal heat loss, safety, and environmental protection [26]. Hence, hydrated salt materials exhibit dual-phase heat storage capabilities, encompassing phase changes and thermochemical processes. This facilitates efficient heat storage and release, making them well-suited for thermal management under normal battery operating conditions and enhancing thermal safety measures. The dehydration and hydration of the hydrated salts can be described by the following reversible reactions [20]:

$$Salt \cdot (x+y)H_2O_{(s)} + Q \xleftarrow{dehydration/hydration} Salt \cdot (x)H_2O_{(s)} + yH_2O_{(l/g)} \quad (1)$$

Numerous scholars have extensively studied the mechanisms and properties of hydrated salt materials, providing substantial evidence of their promising applications [27–32]. From these

studies, $Na_2SO_4 \cdot 10H_2O$ stands out with a phase transition temperature suitable for the LIB temperature control range and a higher enthalpy value. Liu et al. [33] pointed out that $Na_2SO_4 \cdot 10H_2O$-$Na_2HPO_4 \cdot 12H_2O$ eutectic hydrated salt with a melting temperature of 31.2 °C exhibits no phase separation phenomenon and demonstrates good thermal stability after 200 thermal cycles. However, despite progress in experimental research on numerous hydrated salt materials, there has been limited exploration in applied studies. Man et al. [34] conducted a comprehensive review of the advancements in improving the thermal performance of inorganic salt hydrate PCMs. The highlighted challenges include high undercooling, phase separation, leakage susceptibility, low thermal conductivity, and instability, along with measures to enhance the thermal conductivity and stability of PCMs. Hydrate salt materials are extensively used in diverse fields, including heat exchangers and solar photovoltaic-thermal systems [35]; however, research on their application in BTMS is scarce.

Previous studies on the application of hydrated salt materials to BTMS have primarily focused on their phase transition processes. However, in-depth studies have been conducted on the dehydration processes. Zhu et al. [36] present a new PCM with $KAl(SO_4)_2 \cdot 12H_2O$ and $Na_2SO_4 \cdot 10H_2O$ as raw materials, effectively maintaining the battery temperature below 60 °C for 1903 s at 6 W. Ping et al. [37] utilized the phase change process of $Na_2HPO_4 \cdot 12H_2O$ encapsulated with silica as the encapsulation matrix, revealing its outstanding cooling performance and effective mitigation of TR. Ling et al. [38] developed an inorganic PCM of SAT-Urea, confirming its non-flammability and long-term stability, thereby providing a cooler and more uniform thermal environment for LIB. Although hydrated salt PCMs demonstrate effective cooling capabilities for LIB during regular operation, they fall short of storing the significant heat generated during TR initiation. Additionally, PCMs with high thermal conductivity may exacerbate the situation by accelerating the heat transfer to neighboring cells, leading to the spread of TR. Lin et al. [22] proposed SAT-urea/ expanded graphite (EG) as a thermal management material that combines latent heat and thermochemical storage and examined its impact on TR propagation. Cao et al. [24] conducted numerical simulations of penetration-induced TR propagation in battery packs, both with and without composite phase change material (CPCM), and demonstrated that SAT/EG effectively prevented TR propagation by absorbing and storing heat in two stages of heat storage. Dai et al. [2] proposed an inorganic PCM with nonflammability that has the potential to achieve a dual function, working as a TR barrier, which effectively mitigated TR and TR propagation. These innovative studies provided a basis for the use of hydrated salt materials in TR applications. Nevertheless, as mentioned above, the melting points of the PCMs typically exceed 50 °C, rendering them unsuitable for the optimal operating temperature range (20–40 °C) crucial for thermal control in LIB.

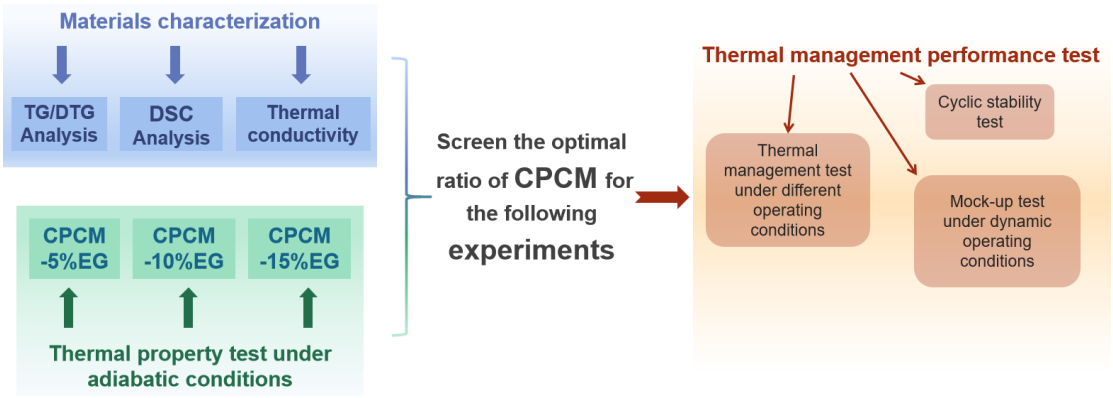

Fig. 1. Research roadmap of this paper.

Based on the abovementioned research gaps, to provide multi-stage thermal management at reasonable temperatures, this study proposes a novel hydrated salt CPCM comprising $Na_2SO_4 \cdot 10H_2O$ and $Na_2HPO_4 \cdot 12H_2O$ as the core PCM, carboxymethyl cellulose (CMC) as a thickening agent, and EG as the thermal conductivity enhancer. The proposed CPCM demonstrates a two-stage temperature control function applicable to battery thermal management (BTM) and thermal safety protection. The experiment followed the roadmap illustrated in Fig. 1. Initially, CPCMs with varying mass fractions of EG were characterized, conducting thermogravimetric (TG)/differential thermogravimetric (DTG) tests, differential scanning calorimeter (DSC) tests, and thermal conductivity measurements separately. Based on the characterization analysis and thermal property tests, the optimal mass ratio for CPCM is determined, revealing a melting point of 29.05 °C, a latent heat of 183.7 $J \cdot g^{-1}$, and a high thermal conductivity of 3.926 $W \cdot m^{-1} \cdot K^{-1}$. Compared to existing PCMs, it exhibits phase transition temperatures more suitable for LIBs and superior thermal control effects. In addition, a schematic of the heat storage process for the CPCM describes the operational principles of the multistage heat storage process. In subsequent experiments, the CPCM was employed for high-rate discharging and TR tests, with a focus on validating its cyclic stability. Specifically, to investigate the impact of CPCM on the thermal control of LIB in practical scenarios, we introduce dynamic operating condition experiments for LIB. The experimental results indicated that CPCM's two-stage temperature control performance of the CPCM plays a vital role in BTMS and TR mitigation.

2.Materials preparation and characterization

Section 2.1 outlines the material preparation process, while Section 2.2 introduces the experiments for material characterization.

2.1Materials preparation

Section 2.1.1, describes the raw materials used for the preparation of CPCM and in section 2.1.2 the process of CPCM preparation is described.

2.1.1Raw materials

A CPCM consisting of inorganic hydrated salts and additional substances was prepared. The CPCM comprised sodium sulfate decahydrate (SSD), disodium hydrogen phosphate dodecahydrate (DHPD), CMC, and EG. The SSD ($Na_2SO_4 \cdot 10H_2O$, purity ≥ 99%, analytical reagent) and DHPD ($Na_2HPO_4 \cdot 12H_2O$, purity ≥ 99%, analytical reagent) were utilized as inorganic hydrated salt PCMs, with melting points of 32.4 and 35 °C. CMC was also used as a thickening agent. All reagents were purchased from Beijing Innochem Technology Co., Ltd. The EG (80 mesh, carbon content: 99%) was provided by Qingdao Graphite Co., Ltd., China. Icosane (purity ≥ 99%, phase transition temperature 36.8 °C) was obtained from Guangdong Wengjiang Chemical Reagent Co., Ltd.

2.1.2 Preparation of CPCM

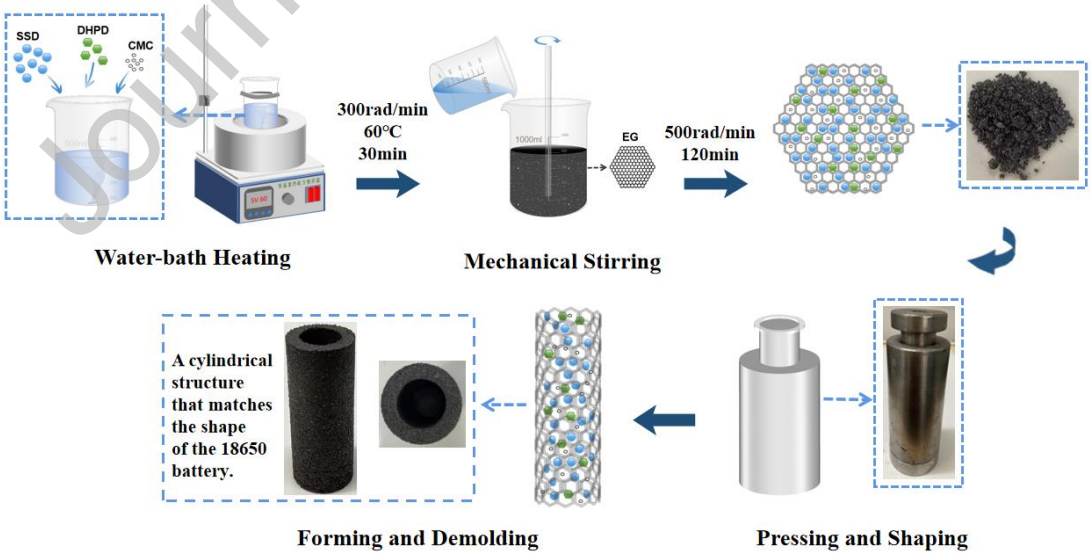

Fig. 2. Preparation and shaping process of composite phase change material (CPCM).

Considering the suitable melting temperature for BTM, binary eutectic hydrated salt (composed of 80%$Na_2SO_4 \cdot 10H_2O$ and 20%$Na_2HPO_4 \cdot 12H_2O$), with excellent performance, was chosen as the inorganic hydrated salt PCM. This salt is expected to eliminate phase separation, as predicted by the binary eutectic phenomenon and solubility theory [31,32]. The hydrated salt mixture was melted in a beaker in a water bath at 60 °C, forming a binary eutectic hydrated salt. However, severe phase separation of $Na_2SO_4 \cdot 10H_2O$ still occurred continuously, leading to the persistent eutectic salt phase separation. To address this issue, after the addition of 5% CMC relative to the mass fraction of the eutectic salts, the solution was stirred at 300 rpm at a constant temperature for 30 min until complete fusion. This preparation eliminated all remaining phase separations. Subsequently, EG with relative mass ratios of 5%, 10%, and 15% was incorporated into the liquid eutectic salt to address the problems of insufficient thermal conductivity and macroscopic instability of the hydrated salt materials. The composites were mechanically stirred at 300 rpm for 2 h to ensure uniform adsorption of the eutectic hydrated salt in the pores of the EG. Then, three sets of CPCMs were produced using molds to shape cylindrical structures matching the shape of the 18650 LIB (inner diameter 18.5 mm, outer diameter 29.5 mm, thickness 5.5 mm, height 65 mm, and density 1 $g \cdot cm^{-3}$). When prepared with various EG contents, the CPCMs exhibited defined hardness and stable morphology. The three sets were labeled CPCM-5% EG, CPCM-10% EG, and CPCM-15% EG. The preparation process for CPCM is illustrated in Fig. 2.

2.2 Materials characterization

To further investigate the microstructures of EG and CPCM with different EG mass contents, scanning electron microscopy (SEM, APREO 2S, America) was used to observe the microstructures of CPCM-5%EG, CPCM-10%EG, and CPCM-15%EG, and the magnifications were 1,000 times and 10,000 times.

To evaluate the thermal stability and thermochemical heat storage capacity of CPCM with different EG contents, thermogravimetric analysis was conducted using a thermoanalyzer instrument (TGA, NETZSCH, STA449F3, Germany). CPCM samples (8–12 mg) were heated from 30 to 200 °C at a rate of 5 $°C \cdot min^{-1}$ under a nitrogen atmosphere with a flow rate of 20 $mL \cdot min^{-1}$.

The melting point of a phase change material determines its field of application and the enthalpy of the phase change determines its heat storage properties; the greater the latent heat, the greater the heat storage capacity. To obtain the phase-change thermal-storage capacity of the CPCMs with different EG contents, the phase-transition temperature and phase-change enthalpy of the CPCMs were measured using a DSC (NETZSCH, 200F3, Germany). Samples (8–12 mg) were

enclosed within an alumina pan and heated from 10 to 50 °C at a rate of 5 °C·min^{-1} in a purified nitrogen atmosphere.

The thermal conductivity directly affects the heat transfer performance of an energy storage system. To evaluate the effect of EG addition on the thermal conductivity of three groups of CPCMs and analyze the change of thermal conductivity between solid-state and molten-state CPCMs, thermal conductivities of both solid- and molten-state CPCMs were measured using the hot-plane method at 25 and 40 °C on a thermal constant analyzer (Hot Disk TPS2500S, Sweden). Before the measurement, three sets of CPCM samples were compressed to form 3.5 × 6.7 cm slices with a thickness of 1 cm and density of 1 g·cm^{-3}. The uncertainty in the thermal conductivity measurement was ± 3%.

Following the initial characterization tests, we compared the thermal properties of materials with varying EG mass contents to guide the final material selection.

3.Experiments

Section 3.1 explains the battery thermal characterization, Section 3.2 describes its application in adiabatic thermal property experiments, and Sections 3.3 and 3.4 elaborate on the procedures for the thermal management and TR experiments.

3.1 Battery thermal characterization

To ensure safety and facilitate better control over battery heating rates, we selected a heating rod (i.e., test battery) of the same size as the 18650 LIB (φ 18 × 65 mm). This rod had a resistance value of 170 Ω and was connected to a programmable DC power supply (DC, NGI, N3600, China) for heating. This setup simulates the heating experienced by the LIB during charging and discharging. According to our previous study [9], the heat generation rate of LIB can be expressed as a quadratic function of the charge-discharge rate. Furthermore, the charge/discharge heat generation rate decreases with increasing temperature at ambient temperatures of 15, 25, and 35 °C. As illustrated in Fig. 3, the heat-generation rate was fitted using the quadratic polynomial function $f(x)=ax^2+bx+c$. The fitting results are listed in Table 1. The table also provides the corresponding relationship between the charge/discharge rate and heating power at various ambient temperatures, as utilized in the subsequent experiments.

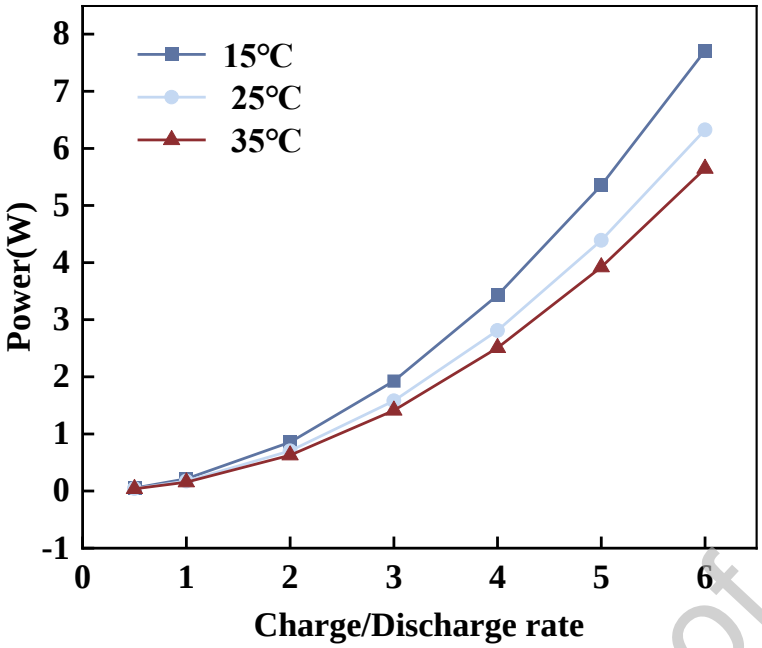

Fig. 3. Correlation between the charge/discharge rate and the heat generation rate in various ambient temperatures

Table 1 Fitting results and corresponding relationships between heating power and discharge rate.

Ambient temperature (°C)	a	b	c	3 W	8 W
15	0.2142	−1.2280e-4	2.5745e-15	3.742C	6.111C
25	0.1757	−1.2280e-4	2.7063e-15	4.132C	6.748C
35	0.1568	−1.2280e-4	2.6781e-15	4.374C	7.143C

3.2 Thermal property test under adiabatic conditions

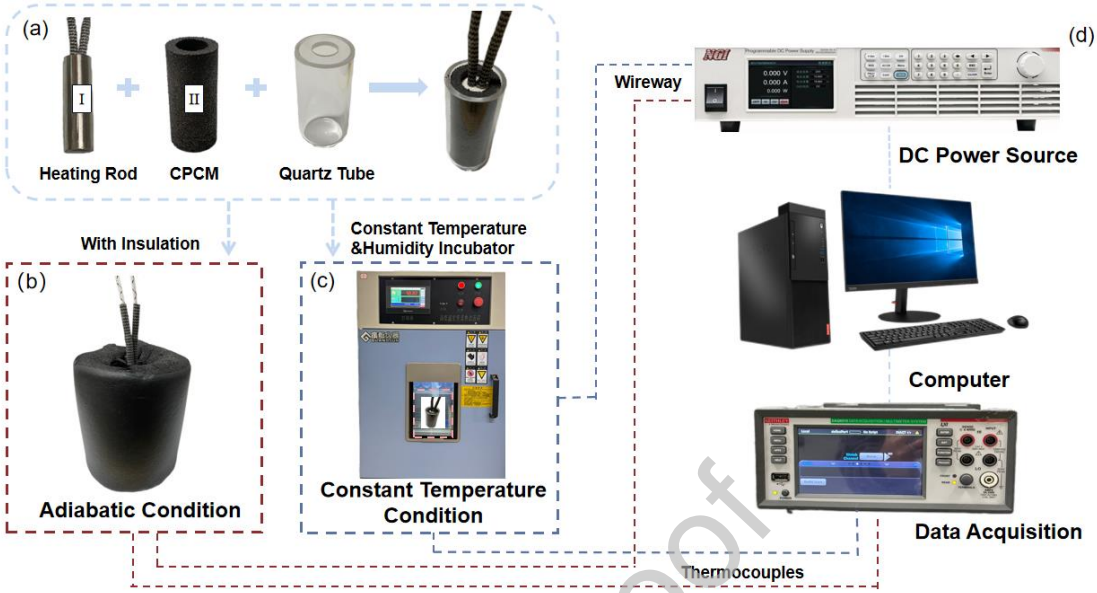

Fig. 4. Schematic diagram of the experimental setup.

The experimental design is illustrated in Figs. 4(a)−(d). Standardized characterization materials were employed to investigate the thermal properties of passive thermal management and their effectiveness in temperature control. To assess the temperature control effects of the CPCMs with varying EG contents on the test batteries, we established a relatively adiabatic external environment and recorded the observed temperature changes. The optimal mass ratio of the CPCMs was determined by comparing the characterization parameters for subsequent research. Initially, the K-type thermocouple I was affixed to the surface midpoint of the test battery. Subsequently, a cylindrical CPCM with a thickness of 5.5 mm was placed on the exterior of the test battery and K-type thermocouple II was attached to the midpoint of the outer surface of the CPCM. These thermocouples were connected to a temperature data acquisition instrument (DAQ6510, Keithley, America) to record the temperatures inside (i.e., the surface of the test battery) and outside the CPCM. The CPCM and test battery were enclosed inside a high-temperature-resistant quartz tube with an inner diameter of 30 mm. The quartz tube was securely covered with a 5 cm insulating layer to establish a relatively insulated environment.

In the blank control experiment, the test battery was positioned within a quartz tube devoid of CPCM and the surface temperature was measured. The current and voltage of the DC power supply are regulated to simulate the heating capability of the test battery. The heating of the LIB during high-C-rate discharging was simulated by applying 3 and 8 W to the test battery, while the heating

behavior of the TR was simulated by applying 100 W. The cutoff temperature was set at 130 °C, at which point heating ceased when the temperature outside the CPCM reached 130 °C.

3.3 Thermal management performance test

The optimal CPCM determined in Sections 2.2 and 3.2 was used for the subsequent thermal management experiments. The experimental setups are illustrated in Figs. 4(a)−(d). In contrast to the experiment described in Section 3.2, we employed a constant temperature and humidity incubator (GTJ-G, Guangjun Testing Instrument Co., Ltd.) to establish diverse ambient temperatures.

3.3.1 Thermal management test under different operating conditions

In addition to the blank control experiment, this section includes a controlled experiment using icosane as the phase change material for comparative analysis. Temperature measurements were taken on the battery surface and the outside of the materials at ambient temperatures of 15, 25, and 35 °C, along with 3 and 8 W heating. The effectiveness of temperature control was evaluated based on the maximum temperature (T_{max}) and the maximum temperature difference (ΔT_{max}) of different CPCM materials.

3.3.2 Cyclic stability test

To investigate the cyclic stability of CPCM-10%EG, the experiments in this section revolve around the temperature-control performance of CPCM-10%EG heated over multiple cycles. The test cell was tested in 10 heating-shelving cycles at an ambient temperature of 25 ° C. In each cycle, the simulated cell was heated at 3 W for 20 min and then set aside for 60 min and the temperature changes between the inner and outer sides of the CPCM-10%EG were recorded using a temperature data collector, with 2 min as the temperature measurement interval. The cycling stability of the CPCM-10%EG was evaluated based on the maximum surface temperature (T_{max}) and maximum inner and outer temperature difference (ΔT_{max}) of the test battery during each cycle.

3.3.3 Mock-up test under dynamic operating conditions

The experiments in the previous section considered the LIB as a constant heat source and focused on the temperature change of the LIB under a constant discharge rate. However, the charge/discharge rate of the LIB in real work will continue to change and it is in a dynamic working condition, which makes the temperature change more complicated. In this section, three dynamic

high-rate charge/discharge cycles are set up to further evaluate the temperature control effect of the CPCM-10%EG under dynamic working conditions in combination with the LIB under real working conditions. The dynamic working conditions included higher-rate (2C) charging, different high-rate discharging (3, 5, 7C), and five working conditions of shelving, simulating the real LIB in the working scene. The test unit was placed in a constant temperature and humidity chamber and the experiments were carried out at 15, 25, and 35 °C, respectively, with a DC power supply connected to a temperature data collector and a temperature measurement interval of 2 min.

3.4 Mock-up test of TR

To evaluate the temperature control effect of CPCM-10%EG on the TR of the battery under different ambient temperatures, we conducted an experiment in which the test battery was heated with 100 W power [24] to simulate the warming of the LIB in the TR state. For comparison, we also tested the battery protected by eicosane as a phase change material and conducted a control experiment without temperature control material protection. The experiments were carried out in a constant temperature and humidity chamber. Due to the drastic temperature change, the temperature measurement interval was 10 s.

4. Results and discussions

Sections 4.1 and 4.2 present the thermal performance results and use them to determine the optimal CPCM; Sections 4.3 discusses the impact of temperature control, which is crucial for the thermal management experiments; and Section 4 discusses the TR experiment results.

4.1 Characterization analysis of CPCMs

In this section, according to Section 2.2, the characterization results of CPCMs with different EG mass contents are discussed, including SEM, TG/DTG, DSC, thermal conductivity analysis, and thermal storage principle of the CPCM.

4.1.1 SEM analysis

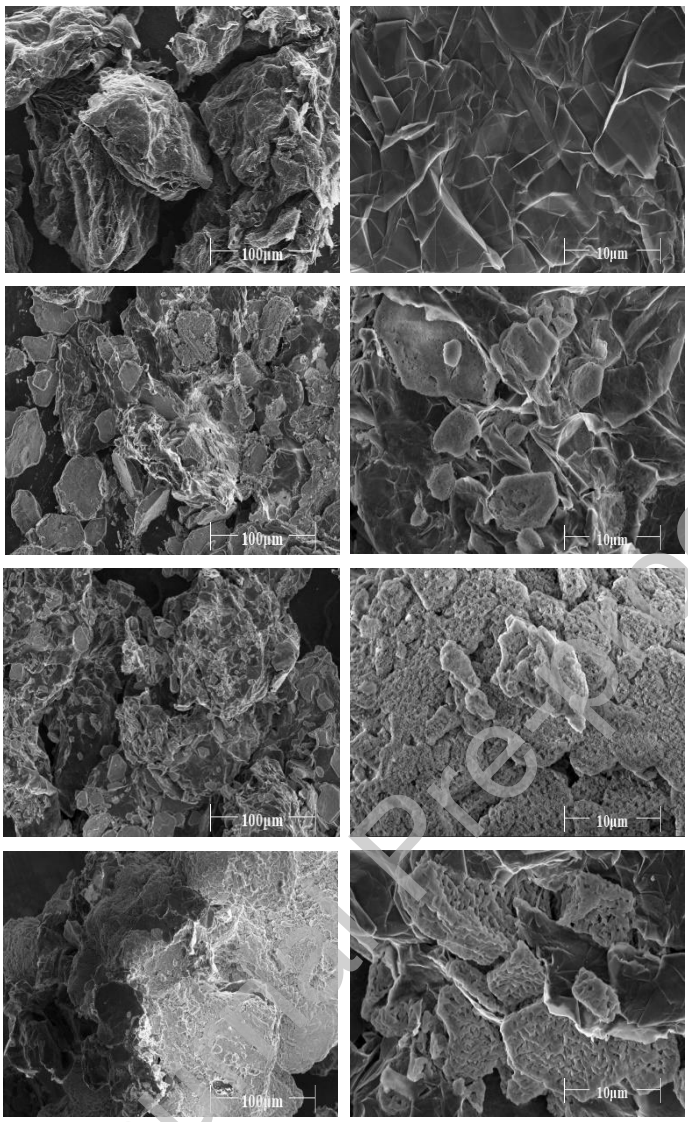

Fig. 5. (a) and (b) scanning electron microscopy (SEM) of expanded graphite (EG) and composite phase change material (CPCM) with different EG mass contents: EG; (c) and (d) CPCM-5% EG; (e) and (f) CPCM-10% EG; and (g and h) CPCM-15% EG.

To further understand the microstructure of the CPCM with different EG mass contents, SEM analysis was conducted on the EG, CPCM-5% EG, CPCM-10% EG, and CPCM-15% EG samples at the magnification of 1,000 times and 10,000 times. The observations of EG and the three CPCM structures provided a more intuitive understanding of the distribution of hydrated salts with EG. Fig. 5(a) depicts the original form of the EG material, which resembles worm-like graphite with

numerous pores. In Fig. 5(b), the more microscopic view of EG reveals a distinct layered structure that accommodates a substantial amount of PCMs. Figs. 5(c)–(h) show the distributions of the binary eutectic hydrated salt within the pores of EG. As the EG content increased and relative content of the eutectic hydrated salt decreased, the pores of EG gradually became less filled. In CPCM-5% EG, eutectic salt particles accumulated in large quantities on the surface of the EG and could not fill the pores, leading to pore clogging in the EG skeleton. However, in CPCM-15% EG, the pores were not filled, resulting in a lower utilization rate of EG and subsequent reduction in the overall heat storage density. Conversely, in CPCM-10% EG, the eutectic salt and CMC were uniformly distributed within the pores and covered the EG surface; therefore, too little EG addition (5%) will cause a large amount of the remaining hydrated salt to be unable to be adsorbed by the EG, increasing the overall thermal resistance. Moreover, excessive addition of EG (15%) will result in more EG being unable to play a role, thus reducing the overall thermal storage density of the material will be reduced. From a microscopic perspective, the addition of 10% EG was more suitable for the modification of CPCM.

4.1.2 TG/DTG analysis

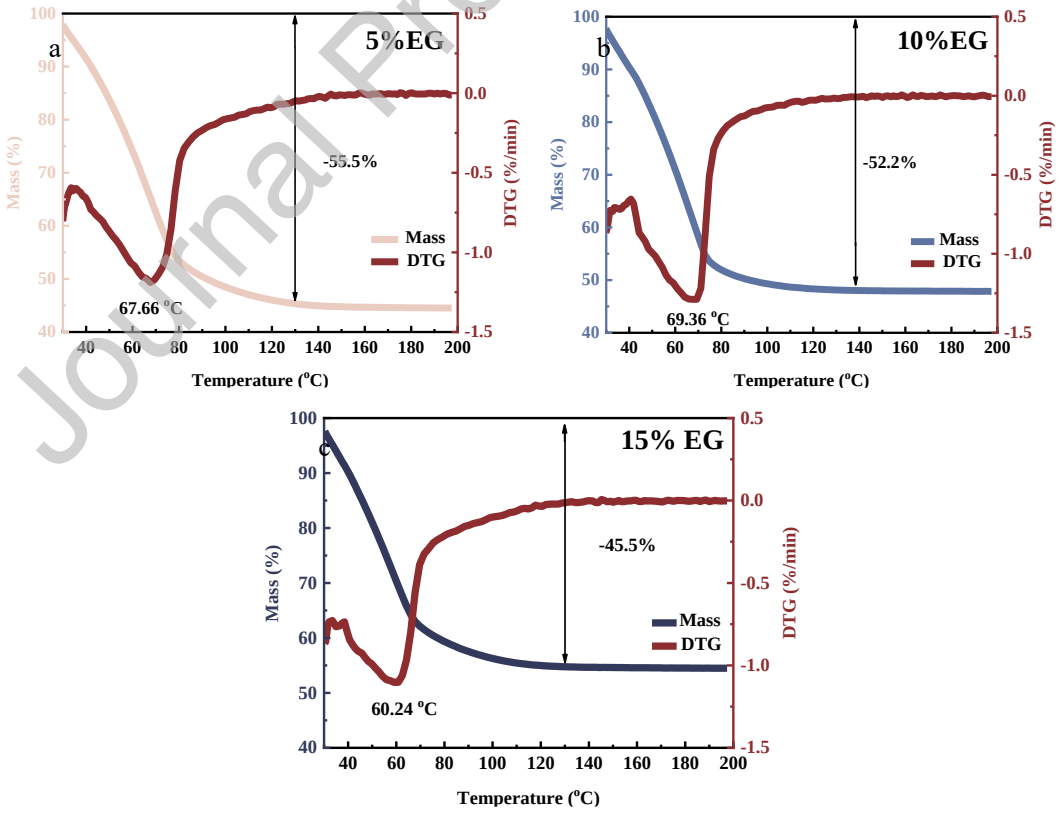

Fig. 6. Thermogravimetric (TG) and differential thermogravimetric (DTG) curves of (a) composite phase change material (CPCM)-5%EG; (b) CPCM-10%EG; and (c) CPCM-15%EG.

The thermal stabilities of the three groups of CPCMs were assessed through TG analysis, and the corresponding results are shown in Figs. 6(a)−(c). The TG and DTG curves depict the relationship between the mass change of the CPCMs with varying EG content and temperature. Within the entire temperature range, the samples exhibited a single mass loss; as the EG content increased from 5% to 15%, the mass losses were 55.5%, 52.2%, and 45.5%. This decrease was attributed to a reduction in the hydrate salt content and amount of dehydration. Notably, the mass loss of CPCMs is concentrated from 40 to 100 °C, potentially resulting from the release of moisture and dehydration of hydrated salts. The mass loss rates of CPCM with 5%, 10%, and 15% EG reach their maximum at 67.66, 69.36, and 60.24 °C, respectively. The mass of CPCM remains constant when the temperature reaches 130 °C, indicating the completion of dehydration. Table 2 lists the theoretical dehydration values for the three sets of CPCMs, calculated using the following equation:

$$Theoretical\,\Delta m = \frac{M_{H_2O}}{M_{CPCM}} \quad (2)$$

where M is the molar mass of the corresponding substance. The actual dehydration values were lower than the theoretical values because of water dissipation caused by the heating and stirring steps during preparation.

Table 2 Mass changes of CPCMs with different EG contents

Parameters	CPCM-5%EG	CPCM-10%EG	CPCM-15%EG
Actual Δm (%)	55.5	52.2	45.5
Theoretical Δm (%)	58.2	53.3	48.9

4.1.3 DSC analysis

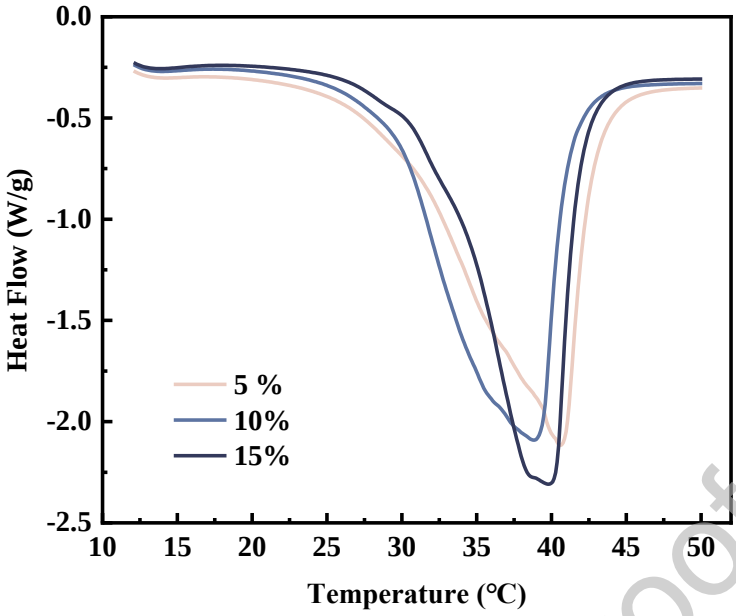

Fig. 7. Differential scanning calorimetry (DSC) curves of composite phase change materials (CPCMs) .

As shown in Fig. 7, DSC analysis was used to investigate the phase-change properties of the CPCMs with EG contents of 5%, 10%, and 15%. Detailed data are presented in Table 3. The melting point of phase change materials delineates their applications, whereas the enthalpy of the phase change significantly influences thermal energy storage. Higher latent heat contributes to a more robust thermal storage capacity. EG plays a dual role. It acts as a heat transfer enhancer and combines with hydrated salts to form a CPCM, thereby enhancing the thermal conductivity of phase change materials, and functions as a porous medium, improving macroscopic stability and preventing leakage, thus ensuring overall structural stability.

All three types of CPCM samples exhibited a peak in their DSC curves, confirming the phase-change thermal storage process of CPCM. The melting points of CPCM with 5%, 10%, and 15% EG were 27.66, 29.05, and 32.62 °C respectively, appropriately catering to the thermal management of LIB. Meanwhile, the phase change enthalpy values decrease to 184.5 $J \cdot g^{-1}$, 183.7 $J \cdot g^{-1}$, and 172.2 $J \cdot g^{-1}$ due to the reduced number of practical phase-change components. However, these levels remain relatively high, ensuring effective heat absorption. Only 1.2 $J \cdot g^{-1}$ of latent heat was lost as the EG content increased from 5% to 10%, indicating that adding 10%EG was suitable for modifying the binary eutectic hydrated salt in this study.

Table 3 Melting temperature and phase change enthalpy of CPCMs.

Parameters	5%EG	10%EG	15%EG
Melting point (°C)	27.66	29.05	32.62
Phase change enthalpy ($J \cdot g^{-1}$)	184.5	183.7	172.2

4.1.4 Thermal conductivity analysis

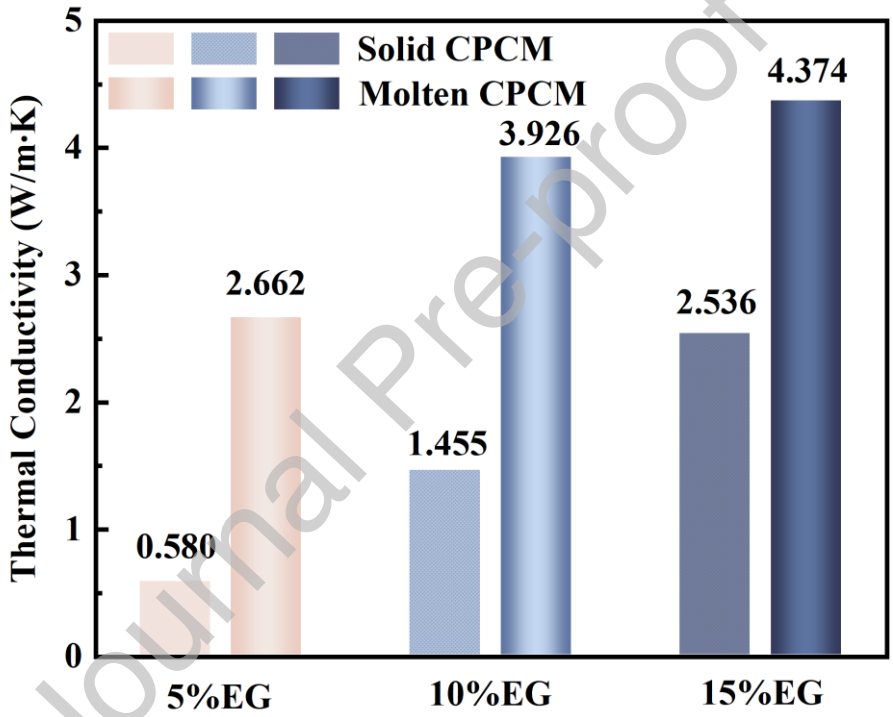

Fig. 8. Thermal conductivities of CPCMs under solid state and molten state.

Fig.8 illustrates the impact of EG on the thermal conductivity of the solid CPCM at 25 °C and molten CPCM at 40 °C. Thermal conductivity plays a pivotal role in determining the heat transfer performance of energy storage systems. The thermal conductivity of pure hydrated salt is approximately 0.5 $W \cdot m^{-1} \cdot K^{-1}$ [34], emphasizing the need for enhancement. The addition of EG substantially improved the thermal conductivity 5–9 times, with further enhancement observed as the EG content increased. Furthermore, the thermal conductivity of molten CPCM surpassed that of solid CPCM, which is attributed to the filling of the EG pores as the binary eutectic hydrated salt melts, thereby reducing the overall thermal resistance.

A comprehensive comparison of the CPCM characterization results revealed a direct correlation between increasing the EG content and enhanced thermal conductivity, albeit at the expense of reduced latent heat values. A tradeoff between high thermal conductivity and high latent heat was evident. During the transition from 5% to 10% EG, the thermal conductivity increases by 47.5%, whereas the enthalpy decreases by 0.6%. However, in the transition from 10% to 15% EG, the thermal conductivity increased by only 11%, whereas the enthalpy decreased significantly by 6.7%. Based on the characterization results, CPCM-10%EG outperformed the other two CPCM formulations, boasting a melting point of 29.05 °C, phase change enthalpy value of 183.7 $J \cdot g^{-1}$, and high thermal conductivity of 3.926 $W \cdot m^{-1} \cdot K^{-1}$.

4.1.5 Thermal storage principle of CPCM

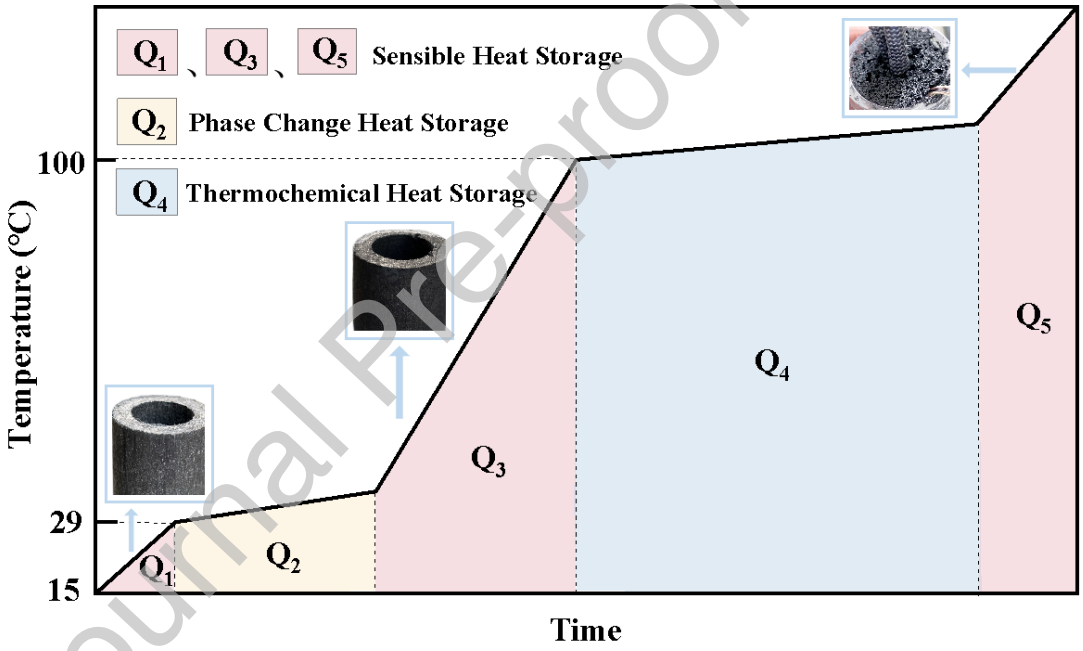

Fig. 9. Schematic diagram of the heat storage process in composite phase change material (CPCM) .

Fig. 9 illustrates the analysis of the heat storage process of the CPCM, including sensible heat storage, phase-change heat storage, and thermochemical heat storage, based on the TG/DTG and DSC test results and in combination with [24]. The corresponding CPCM images at each stage are presented.

Stage I: sensible. As the temperature of the CPCM increased from the initial temperature (15 °C) to the melting point (29 °C), heat was absorbed as sensible heat (Q_1), leading to a rapid temperature increase. During this stage, the CPCM maintained a relatively stable solid form.

Stage II: Phase change. Upon reaching the melting point (29 °C), the temperature increased slowly, exhibiting a phase-change plateau that persisted for some time. Throughout the phase-change process, the CPCM stored a significant amount of heat in the form of latent heat (Q_2).

Stage III: sensible. After the hydrated salt in CPCM completely melted, heat was absorbed again as sensible heat (Q_3), causing the temperature to rise rapidly. During this stage, the molten hydrated salt was evenly adsorbed in the EG pores, rendering CPCM relatively soft. The CPCM remained solid macroscopically and did not leak or sustain damage owing to the porous EG skeleton.

Stage IV: thermochemical. When the temperature of the CPCM reached 100 °C, it underwent dehydration, and vapor rapidly escaped from its pores, absorbing large amounts of heat in the form of thermochemical heat (Q_4). This resulted in a prolonged dehydration plateau, during which the temperature increased minimally.

Stage V: sensible. After dehydration, the temperature rose sharply again and heat was stored as sensible heat (Q_5). During this stage, the CPCM became porous, losing approximately half its mass owing to water loss in the hydrated salt.

4.2 Thermal properties of CPCM with different EG contents

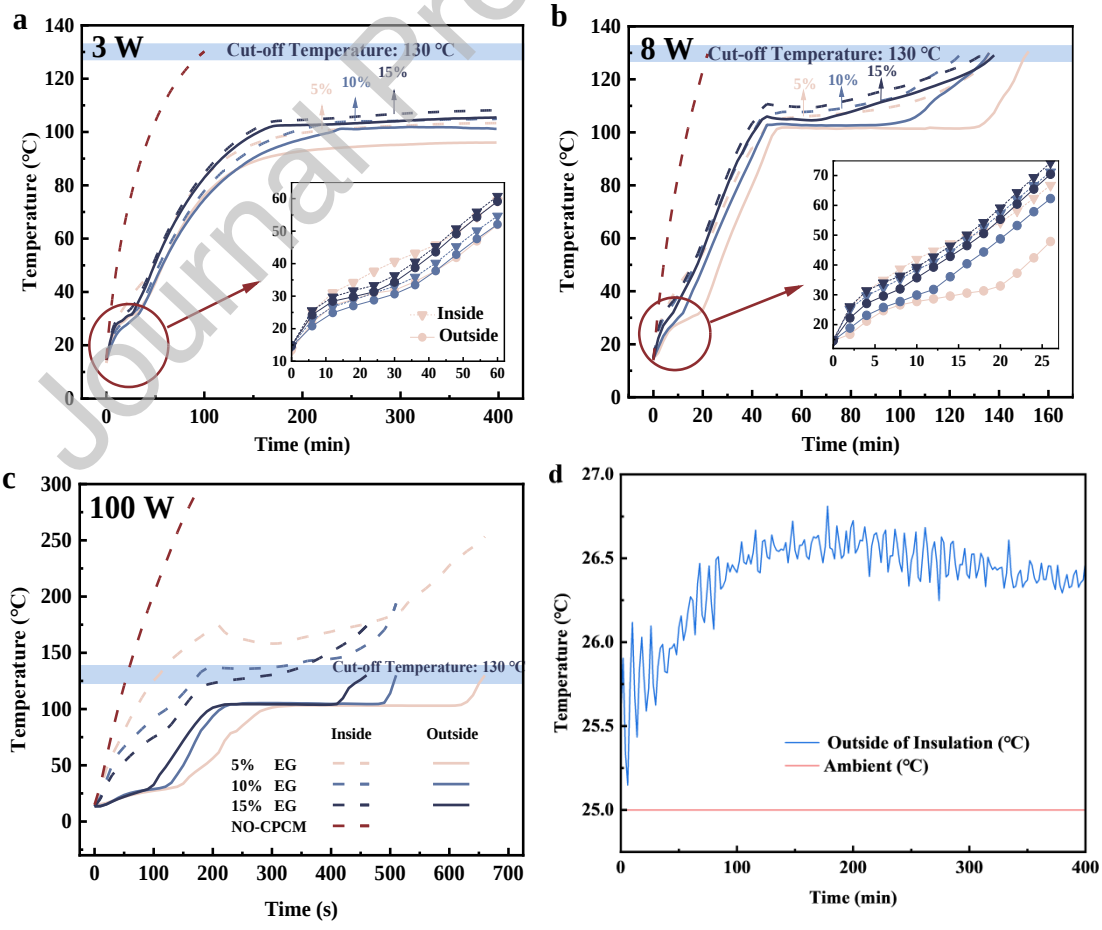

Fig. 10. Temperature with different EG contents under adiabatic conditions: Heating power of (a) 3 W, (b) 8 W, and (c) 100 W and temperature on the outside of the insulating layer at 3 W (d).

Section 4.1 determined that CPCM-10% EG exhibited a more robust performance; however, it did not definitively prove that it was the optimal CPCM for LIB thermal management and thermal safety protection. According to Section 3.2, the test battery's surface was encased in a 5.5 mm thick CPCM and an adiabatic environment was established to evaluate the thermal properties of the CPCMs on the test battery under different heating powers.

The temperature curves on the surface of the test battery (i.e., inside of the CPCM) and outside of the CPCM under adiabatic conditions were simulated using the test battery, as illustrated in Fig. 10(a). Heating of the LIB at a high discharge rate was simulated at 3 W. Without the CPCM, the temperature of the test battery rose rapidly, reaching 130 °C at 100 min. However, with the protection of the CPCM, the heat generated by the test battery was absorbed. The temperature rise process can be categorized into four stages: Stages I–IV of Section 4.1.5. Stage V was omitted because the insulation layer cannot achieve complete adiabatic. Fig. 10(d) shows the temperature outside the insulating layer, which was used to evaluate its insulation effect. The final temperature was maintained at approximately 26.5 °C, only 1 °C higher than the initial temperature of 25.5 °C. At this time, the heat dissipation Φ was about 0.0735 W, indicating a better adiabatic effect. Consequently, the experimental setup reached thermal equilibrium with the environment once a specific temperature stage was attained, preventing further increases in the temperature. After reaching the melting point of CPCM at approximately 29 °C, the phase-change temperature plateaued for 20–40 min. When the temperature of CPCM reached 100 °C for dehydration, a substantial amount of heat was extracted due to vaporization and vapor escape, maintaining the temperature below 115 °C.

As shown in Fig. 10(b), the test battery at 8 W simulated the heat generation of the LIB under high-rate discharge conditions. The test battery reached a temperature of 130 °C within 22 min without the CPCM. However, with the protection of CPCM, the temperature rise process is delineated into the five stages (I–V) outlined in Section 4.1.5. The phase-change plateau persisted for 10–15 min and the dehydration plateau for 20–80 min. The surface temperature of the test battery reached 130 °C after 120 min.

As shown in Fig. 10(c), the heating process of the LIB under TR conditions was simulated at 100 W. The test battery without CPCM rapidly reached a cut-off temperature of 130 °C at 55 s, indicating the rapid development of TR. The results indicated that, without adequate shielding, TR

can quickly propagate to other cells within a battery module, leading to severe consequences. The temperature rise process of the test battery with CPCM was divided into the five stages delineated in Section 4.1.5. Initially, the CPCM melted and absorbed a portion of the heat, mitigating the rate of temperature increase of the test battery before transitioning to the dehydration stage. Due to its impressive thermochemical heat storage capability, it maintained a dehydration plateau for 200–300 s by absorbing a substantial quantity of heat. Furthermore, the results indicated that the CPCM can not only delay the temperature of the test battery from surpassing the safety limit but also effectively postpone the occurrence and spread of TR.

The same trend was observed for the three heating powers. With an increase in the EG content of 5%, 10%, and 15%, the temperature difference between the inside and outside of the CPCM decreased owing to the enhanced thermal conductivity, indicating faster temperature transmission to the exterior. Nevertheless, the corresponding plateaus for phase change and dehydration decreased, which was attributed to the reduced hydrate salt content and consequent enthalpy value. At 3 and 8 W, the CPCM-15%EG set maintained its highest temperature. As shown in Fig. 10(b), the dehydration plateau of CPCM-15% EG lasted only 20 min, which was shorter than those of CPCM-10%EG (50 min) and CPCM-5%EG (80 min). In addition, the surface temperature of the CPCM-5%EG test battery reached 130 °C at 110 s, significantly faster than the other two sets (Fig. 10(c)). The temperature control performance of CPCM-5%EG was insufficient under a high heating power, thereby failing to meet the standards of thermal safety protection. These results underscore CPCM-10%EG as the optimal choice.

4.3 Effect of the CPCM-10%EG on thermal management

The BTM analysis in this section is based on the experimental procedures outlined in Section 3.3.

4.3.1 Thermal management performance comparisons of the CPCM-10%EG and icosane under varying operating conditions

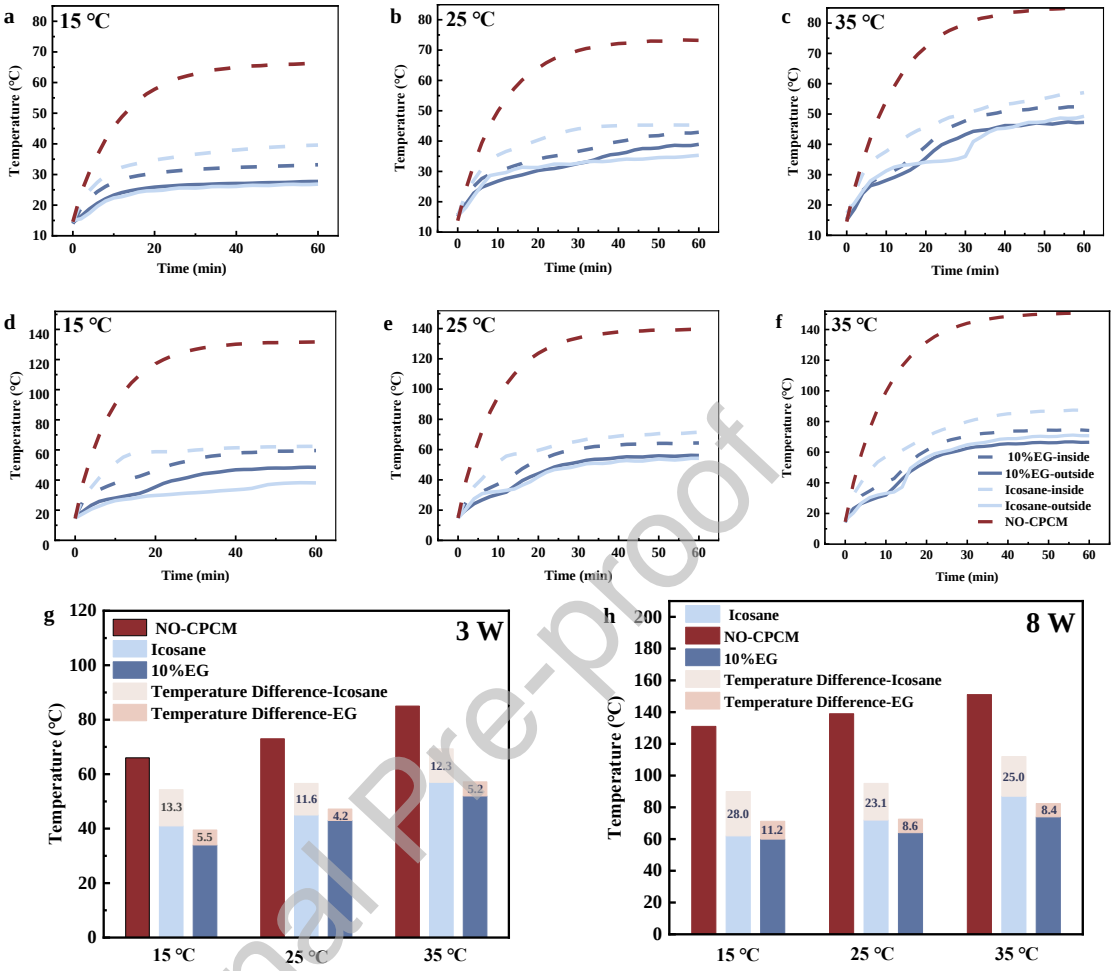

Fig. 11. Comparison of test battery with different temperature control materials under various operating conditions: temperature curves at (a) 3 W, 15 °C; (b) 3 W, 25 °C; (c) 3 W, 35 °C; (d) 8 W, 15 °C; (e) 8 W, 25 °C; and (f) 8 W, 35 °C and T_{max} and ΔT_{max} at (g) 3 W and (h) 8 W.

The experimental results of the material characterization and thermal properties demonstrated the superior performance of CPCM-10%EG. To achieve comparable outcomes, we employed icosane, an organic phase-change material widely employed in BTMS because of its melting point to CPCM-10%EG and high latent heat. The experiment occurred at commonly observed ambient temperatures of 15, 25, and 35 °C. Figs. 11(a)−(f) compare the temperatures in the absence of CPCM, with icosane and with CPCM-10%EG at varying ambient temperatures and heating powers. The temperature difference between the inside and outside of the material was denoted by ΔT:

$$\Delta T = T_{in} - T_{out} \tag{3}$$

Detailed information on the T_{max} of the test battery and ΔT_{max} between the inside and outside materials is presented in Figs. 11 (g) and 11(h) and Tables 4 and 5. The temperature of the test battery increased sharply without CPCM protection until it reached a specific equilibrium level of heat dissipation from its surroundings, as illustrated in Fig. 11 (a). The T_{max} of NO-CPCM reached 66 °C, which is not conducive to the health and safety of batteries. However, using CPCM-10%EG packaging allows for keeping the test battery temperature within the optimal operating range of LIB by maintaining it below 34 °C. Although icosane and CPCM-10%EG effectively reduced the rate of temperature rise, it is worth noting that CPCM-10%EG had a lower T_{max} and ΔT_{max} than icosane under all operating conditions. This can largely be attributed to the higher phase-change enthalpy and thermal conductivity of CPCM-10%EG, allowing for greater heat storage density and faster heat transfer to the environment.

Table 4 Detailed data comparison with different temperature control materials of T_{max}

Environment temperature		15 °C	25 °C	35 °C
3 W	NO-CPCM	66	73	85
	Icosane	41	45	57
	10% EG	34	43	52
8 W	NO-CPCM	131	139	151
	Icosane	62	72	87
	10% EG	60	64	74

Table 5 Detailed data comparison with different temperature control materials of ΔT_{max}

Environment Temperature		15 °C	25 °C	35 °C
3 W	Icosane	13.3	11.6	12.3
	10% EG	5.5	4.2	5.2
8 W	Icosane	28.0	23.1	25.0
	10% EG	11.2	8.6	8.4

4.3.2 Cyclic stability of the CPCM-10%EG

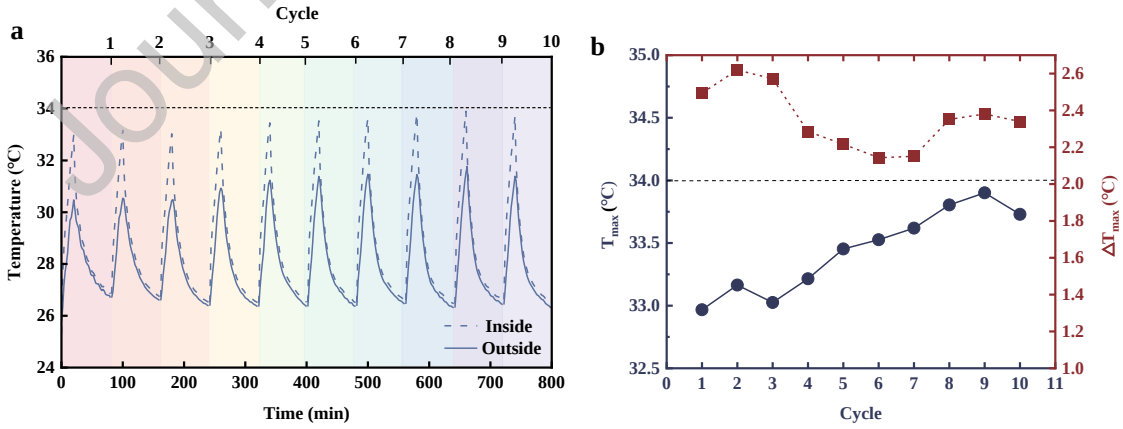

Fig. 12. Stability performance of composite phase change material (CPCM)-10% EG: (a) temperature inside and outside CPCM-10% EG during ten discharge-shelving cycles and (b) T_{max} and ΔT_{max} in each cycle.

In addition to single discharge process testing, CPCM-10% EG exhibited reliable cooling performance during continuous operations. Fig. 12(a) displays the temperature curves over ten discharge-shelving cycles, with T_{max} and ΔT_{max} presented in Fig. 12(b). Throughout these cycles, the temperature of the test battery remained below 34 °C and the variation in T_{max} was less than 0.93 °C. The number of cycles did not significantly affect ΔT_{max} or thermal conductivity. CPCM-10%EG demonstrated impressive cyclic stability, making it suitable for long-term use.

4.3.3 Performance of the CPCM-10%EG under dynamic operating conditions

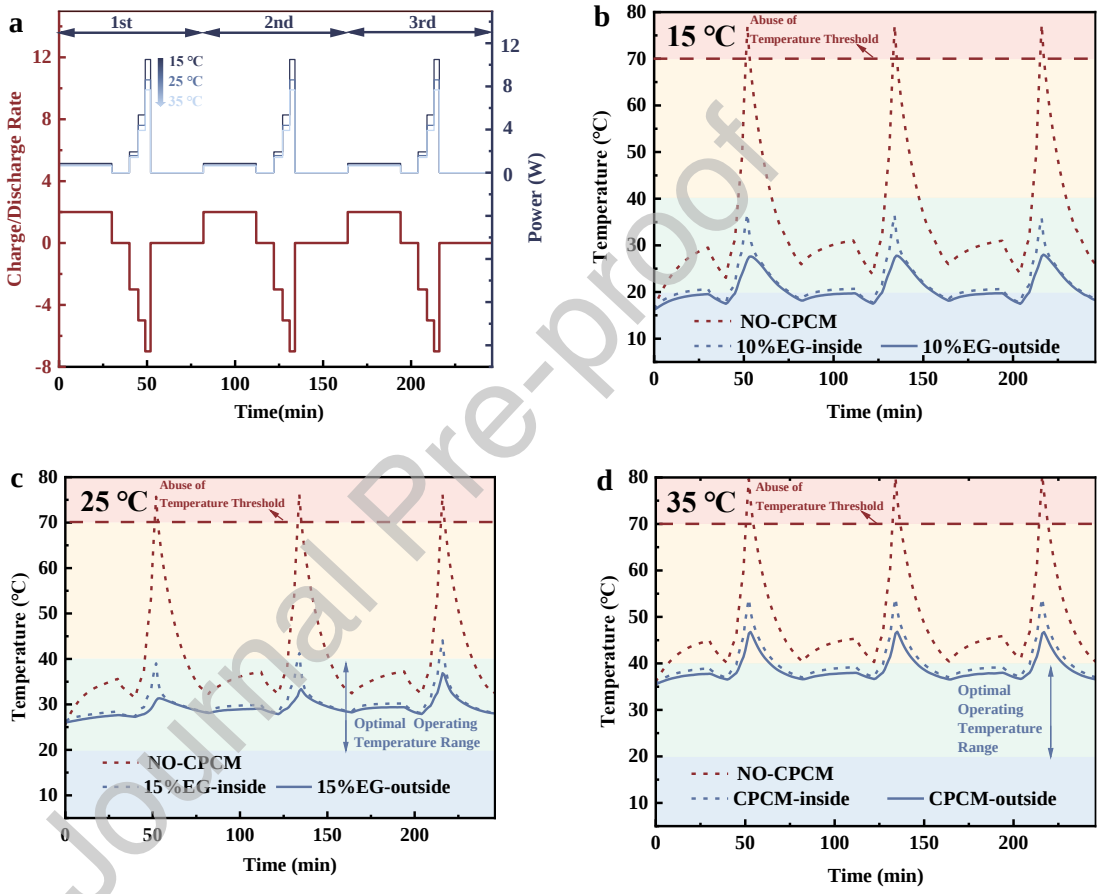

Fig. 13. Performance of the composite phase change material (CPCM)-10%EG under dynamic operating conditions: (a) charging/discharging rate and heating power curves under dynamic operating conditions and temperature with CPCM-10%EG at ambient temperatures of (b) 15 °C, (c) 25 °C, and (b) 35 °C under dynamic operating conditions.

Previous research examined the temperature control effect of CPCM-10%EG on a test battery at a constant heating rate. However, the LIB charge/discharge rate varies frequently in practical scenarios. For instance, the instantaneous discharge rate of electric vehicles can exceed 10C. Previous investigations [2,8,39] generally focused on low discharge rates below 2C. Liu et al.[13]

investigated the thermal equalization behaviors of LIB in a dynamic stress test, which involves a 360-s sequence of power steps, incorporating seven distinct power levels. As a result, we utilized the high discharge rate steps of 3C, 5C, and 7C to study LIB heating during continuous high-rate charging and discharging, which are close to the conditions that trigger TR. To further investigate the effect of CPCM-10%EG on controlling the temperature of the LIB during high-rate charging and discharging under dynamic conditions, the following steps were performed.

(1) Charge at 2C for 30 min;
(2) Shelve for 10 min;
(3) Discharge at 3C for 5 min;
(4) Discharge at 5C for 4 min;
(5) Discharge at 7C for 3 min;
(6) Shelve for 30 min.

These steps were cycled through for all three groups. The correlation between the charge/discharge rate and the heating power in various ambient temperatures determined using Fig. 3 and Table 1 is presented in Fig. 13(a). Particularly, as previously noted, the optimal operating temperature for batteries falls within the range of 20–40 °C. Exceeding this temperature threshold, particularly reaching higher levels beyond 70 °C, poses potential risks such as battery rupture, venting, and electrolyte leakage [3]. Therefore, this study contends that the risk of TR increases when the battery temperature exceeds 70 °C, prompting the establishment of 70 °C as the abuse temperature limit threshold.

The temperature for the dynamic operating step cycle at an ambient temperature of 15 °C is depicted in Fig.13(b). Following discharge at 7C, the test battery without CPCM experiences a temperature increase to 77 °C, surpassing the abuse temperature threshold of 70 °C. This compromises battery health and poses potential safety risks. In contrast, with the protection of CPCM-10%EG, even under the influence of an exceptionally high discharge rate, the peak temperatures during the first, second, and third cycles of the test battery were maintained at 36.7, 36.4, and 35.8 °C, respectively, all falling within the optimal temperature range. Notably, the decline in the peak temperature can be attributed to the fact that during the first cycle at a low ambient temperature, only a small portion of the CPCM was consumed. However, as the cycles progressed, the CPCM gradually melted and absorbed more heat. The higher thermal conductivity of molten CPCM facilitates the transfer of heat to the ambient environment, resulting in a practical cooling effect.

As shown in Fig. 13(c), the test battery temperature with CPCM-10%EG peaked at 39 °C at an ambient temperature of 25 °C during the first cycle, which falls within the optimal temperature range. However, the peak temperature increased as cycling proceeded. Due to the incomplete solidification of CPCM during short-term shelving, it was steadily depleted at higher ambient temperatures.

The results under a high-temperature environment (ambient temperature of 35 °C) are shown in Fig. 13(d). Under the high-temperature conditions, CPCM-10%EG maintained the battery temperature within the optimal operating range only during the 2C and 3C charge and discharge steps. However, the subsequent peak temperature reached 54 °C and remained constant over the three cycles. This is because the CPCM can only absorb heat through sensible heat storage and its effectiveness diminishes when the temperature is controlled in high-temperature environments. Therefore, CPCM-10%EG, with a melting point of 29 °C, is deemed possible but unsuitable for temperature control in high-temperature environments.

4.4 Effect of the CPCM-10%EG and icosane on thermal safety protection

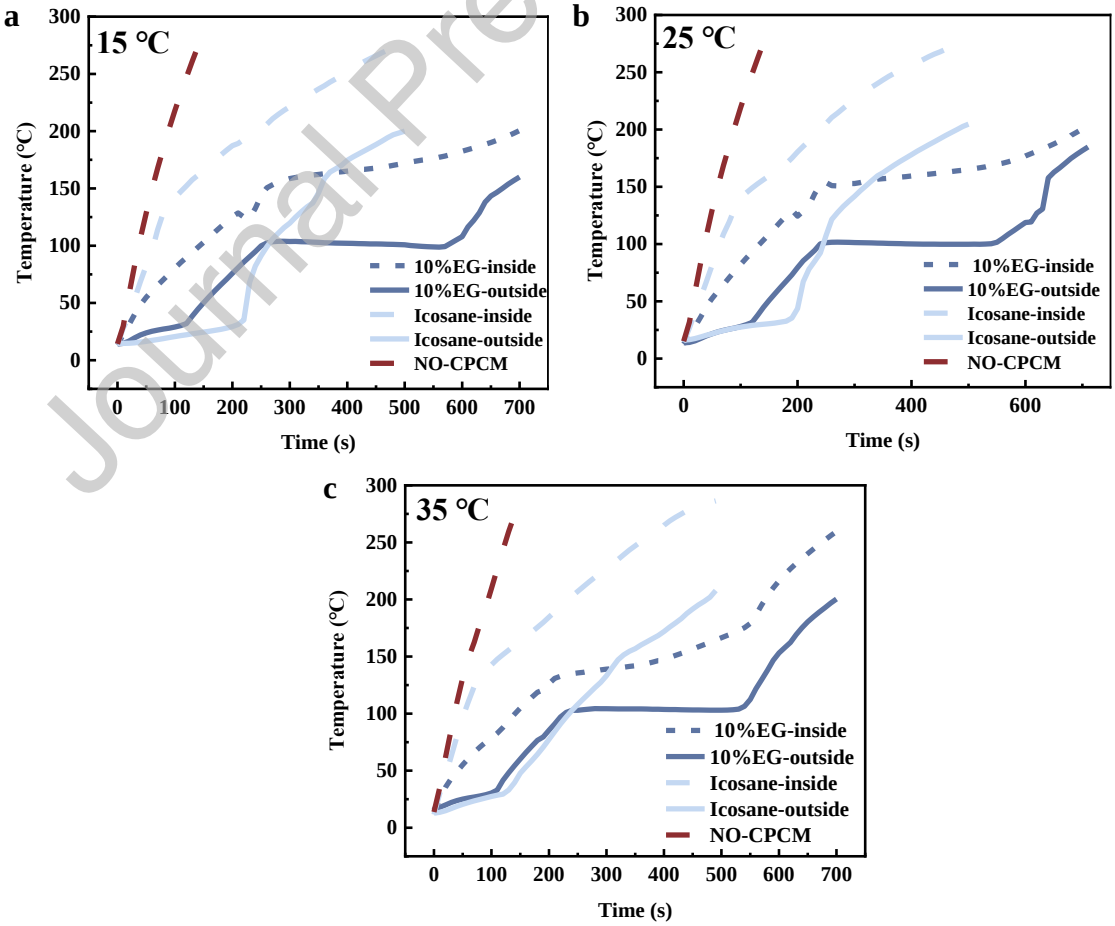

Fig. 14. Temperature with composite phase change material (CPCM)-10% EG and icosane at 100 W under ambient temperatures of (a) 15 °C, (b) 25 °C, and (c) 35 °C.

When a cell is integrated into a module, the initiation of TR in a single cell releases a substantial amount of heat, which is transferred to adjacent cells. This, in turn, triggers a cascade effect of TR within the entire battery module. Therefore, it is imperative to inhibit heat transfer from cells experiencing TR to the external environment. Two primary strategies are employed to mitigate battery TR and its propagation: impeding the heat transfer between cells or employing thermal storage materials to absorb the generated heat [22]. Currently, the prevailing approach to suppress TR and its propagation involves the use of aerogels, which are characterized by exceptionally low thermal conductivity. However, this approach contradicts the conventional belief that an effective BTM requires materials with high thermal conductivity.

Experiments were conducted to investigate whether CPCM-10%EG could contribute to temperature control during TR of LIB at ambient temperatures of 15, 25, and 35 °C using a 100 W test battery. Figs. 14(a)−(c) shows the temperatures of the test battery surface and outside material. The temperature rise exhibited two distinct stages for the case involving icosane, characterized by a notable temperature difference between the test battery's surface and the outside icosane. In the initial stage, the icosane melts and absorbs heat to mitigate the temperature increase. However, owing to its low thermal conductivity, icosane is not highly effective in reducing the battery surface temperature, requiring approximately 80 s to have an impact. At this stage, the surface temperature of the test battery has already surpassed 130 °C. Upon the complete liquefaction of icosane, the temperature outside the icosane surges rapidly and continuously, posing a serious safety threat to the LIB and allowing TR to propagate to adjacent cells. In addition, the ambient temperature was shown to influence the outside temperature. At higher ambient temperatures, the rate of icosane melting increased, whereas the effect on CPCM-10% EG was relatively minor. The temperature increase in the test battery containing CPCM-10% EG occurred in four distinct stages. The first stage involved heat absorption during the phase change of the CPCM, where high latent heat and thermal conductivity effectively delayed the temperature increase. After the initial melting, the temperature of the test battery and the temperature outside CPCM promptly increased until reaching the dehydration threshold of 100 °C. CPCM dehydration, accompanied by the release of vapor that dissipates a significant amount of heat, led to a plateau at a constant temperature outside the CPCM. When the CPCM began to dehydrate, the temperature of the test battery decreased instantly. At ambient temperatures of 15 and 25 °C, the heat absorption of the CPCM effectively cooled the battery temperature by 4.4 °C until the thin layer of the CPCM on the battery surface was fully

dehydrated. The presence of CPCM on the exterior delayed the time required for the test battery surface to reach 130 °C, extending it from 51 to 238 s. In addition, the duration of the dehydration plateau became indistinctively shorter as the ambient temperature increased, reaching 320, 310, and 300 s. This duration provided ample time to prevent heat from being transferred to other cells, allowing for a better reaction time and implementing emergency measures to safeguard the battery module.

5.Conclusions

This paper proposed a novel CPCM tailored for improved BTM and enhanced thermal safety protection, featuring high latent heat, superior thermal conductivity, and a two-stage temperature control mechanism. Extensive characterization and thermal property studies were conducted on the CPCM with varying ratios to determine the optimal amount of EG doping. A series of tests conducted at different discharge rates aimed to demonstrate the efficacy of CPCM in BTM and the mitigation of TR propagation. The key conclusions are as follows:

(1) Material characterization analysis revealed a trade-off between the high enthalpy and high thermal conductivity of the CPCM. CPCM-10% EG exhibited a suitable phase change temperature of 29.05 °C, high latent heat of 183.7 $J \cdot g^{-1}$ and excellent thermal conductivity of 3.926 $W \cdot m^{-1} \cdot K^{-1}$ for effective BTM.

(2) Thermal management experiments demonstrated that CPCM-10%EG reduced the peak temperature from 66 to 34 °C at an ambient temperature of 15 °C and discharge rate of 3.7C. CPCM-10%EG exhibited significantly lower T_{max} and ΔT_{max} than icosane under all operating conditions, allowing for greater heat storage density and rapid heat transfer to the environment.

(3) In 10 discharge-shelving cycles, the test battery temperature stayed below 34 °C, with T_{max} changing by less than 0.93 °C, showcasing the superior cycling stability of CPCM-10%EG. The high-rate charge/discharge dynamic conditions testing indicated the suitability of CPCM-10%EG for practical LIBs, maintaining peak temperatures at 36.7, 36.4, and 35.8 °C over three cycles.

(4) The TR experiments revealed that CPCM-10%EG divided the temperature rise into multiple stages. The thermochemical dehydration slowed the battery temperature increase, increasing the time to reach 130 °C from 51 to 238 s. This suppressed the CPCM outside temperature rise, with the dehydration plateau lasting up to 320 s, preventing further heat transfer to other batteries and TR spread. This ensured the safety of the battery module.

Although this study proposes CPCM-10%EG as a valuable reference for BTMS temperature-control materials, further research on material packaging is essential for practical applications. Future work will explore the application of CPCM-10%EG to various types of LIBs and LIB modules, aiming to contribute to the thermal management and safety of LIBs.

Acknowledgments

The authors would like to thank the National Natural Science Foundation of China (Project No.: 51821004) and the High-level Talent Attraction and Retention Program for Teaching Staff Development at NCEPU.

Nomenclature

Greek	
Δ	Amount of variation
φ	Calibre
Φ	Heat dissipation
Subscripts	
max	Maximum
Acronyms	
LIB	Lithium-ion battery
BTMS	Battery thermal management system
CPCM	Composite phase change material

EG	Expanded graphite
BTM	Battery thermal management
TR	Thermal runaway
EV	Electric vehicle
PCM	Phase change material
SSD	Sodium sulfate decahydrate
DHPD	Disodium hydrogen phosphate dodecahydrate
CMC	Carboxymethylcellulose sodium
SEM	Scanning electron microscopy
TGA	Thermal gravimetric analysis
DSC	Differential scanning calorimeter

References

[1] Q.L. Yue, C.X. He, M.C. et al., Advances in thermal management systems for next-generation power batteries, International Journal of Heat and Mass Transfer 181 (2021) 121853.

[2] X. Dai, P. Ping, D. Kong, et al., Heat transfer enhanced inorganic phase change material compositing carbon nanotubes for battery thermal management and thermal runaway propagation mitigation, Journal of Energy Chemistry 89 (2024) 226–238.

[3] P. Lyu, X. Liu, J. Qu, et al., Recent advances of thermal safety of lithium ion battery for energy storage, Energy Storage Materials 31 (2020) 195–220.

[4] Z. Yu, J. Zhang, W. Pan, A review of battery thermal management systems about heat pipe and phase change materials, Journal of Energy Storage 62 (2023) 106827.

[5] X. Zhang, Z. Li, L. Luo, et al., A review on thermal management of lithium-ion batteries for electric vehicles, Energy 238 (2022) 121652.

[6] Y. Zhao, X. Zhang, B. Yang, et al., A review of battery thermal management systems using liquid cooling and PCM, Journal of Energy Storage 76 (2024) 109836.

[7] A. Väyrynen, J. Salminen, Lithium ion battery production, The Journal of Chemical Thermodynamics 46 (2012) 80–85.

[8] K. Chen, Y. Chen, Z. Li, et al., Design of the cell spacings of battery pack in parallel air-cooled battery thermal management system, International Journal of Heat and Mass Transfer 127 (2018) 393–401.

[9] Q. Liu, L. Qin, Q. Shi, et al., Optimization of the active battery immersion cooling based on a self-organized fluid flow design, Journal of Energy Storage 76 (2024) 109851.

[10] P.V. Chombo, Y. Laoonual, A review of safety strategies of a Li-ion battery, Journal of Power Sources 478 (2020) 228649.

[11] L. Kong, C. Li, J. Jiang, et al., Li-Ion Battery Fire Hazards and Safety Strategies, Energies 11 (2018) 2191.

[12] H. Wang, T. Tao, J. Xu, et al., Thermal performance of a liquid-immersed battery thermal management system for lithium-ion pouch batteries, Journal of Energy Storage 46 (2022) 103835.

[13] Q. Liu, C. Sun, J. Zhang, et al., The electro-thermal equalization behaviors of battery modules with immersion cooling, Applied Energy 351 (2023) 121826.

[14] M. Al-Zareer, I. Dincer, M.A. Rosen, Development and evaluation of a new ammonia boiling based battery thermal management system, Electrochimica Acta 280 (2018) 340–352.

[15] Y. Galazutdinova, S. Al-Hallaj, M. Grágeda, et al., Development of the inorganic composite phase change materials for passive thermal management of Li-ion batteries: material characterization, Int J Energy Res 44 (2020) 2011–2022.

[16] R. Chen, X. Ge, X. Li, et al., Facile preparation method of phase change microcapsule with organic-inorganic silicone shell for battery thermal management, Composites Science and Technology 228 (2022) 109662.

[17] Y.-H. Huang, W.-L. Cheng, R. Zhao, Thermal management of Li-ion battery pack with the application of flexible form-stable composite phase change materials, Energy Conversion and Management 182 (2019) 9–20.

[18] X. Li, J. Deng, Q. Huang, G. et al., Experimental investigation on immersion liquid cooled battery thermal management system with phase change epoxy sealant, Chemical Engineering Science 264 (2022) 118089.

[19] Q. Le, Q. Shi, Q. Liu, X. et al., Numerical investigation on manifold immersion cooling scheme for lithium ion battery thermal management application, International Journal of Heat and Mass Transfer 190 (2022) 122750.

[20] W. Li, J. Jaromír Klemeš, Q. Wang, et al., Efficient thermal management strategy of Li-ion battery pack based on sorption heat storage, Energy Conversion and Management 256 (2022) 115383.

[21] M. Zhi, R. Fan, X. Yang, et al., Recent research progress on phase change materials for thermal management of lithium-ion batteries, Journal of Energy Storage 45 (2022) 103694.

[22] S. Lin, Z. Ling, S. Li, et al., Mitigation of lithium-ion battery thermal runaway and inhibition of thermal runaway propagation using inorganic salt hydrate with integrated latent heat and thermochemical storage, Energy 266 (2023) 126481.

[23] W. Zhang, Z. Liang, X. Yin, et al., Avoiding thermal runaway propagation of lithium-ion battery modules by using hybrid phase change material and liquid cooling, Applied Thermal Engineering 184 (2021) 116380.

[24] J. Cao, Z. Ling, S. Lin, et al., Thermochemical heat storage system for preventing battery thermal runaway propagation using sodium acetate trihydrate/expanded graphite, Chemical Engineering Journal 433 (2022) 133536.

[25] W. Fu, T. Zou, X. Liang, et al., Thermal properties and thermal conductivity enhancement of composite phase change material using sodium acetate trihydrate–urea/expanded graphite for radiant floor heating system, Applied Thermal Engineering 138 (2018) 618–626.

[26] Z. Zeng, B. Zhao, R. Wang, Water based adsorption thermal battery: Sorption mechanisms and applications, Energy Storage Materials 54 (2023) 794–821.

[27] Y. Wu, T. Wang, Preparation and characterization of hydrated salts/silica composite as shape-stabilized phase change material via sol–gel process, Thermochimica Acta 591 (2014) 10–15.

[28] Q. Miao, Y. Zhang, X. Jia, et al., MgSO4-expanded graphite composites for mass and heat transfer enhancement of thermochemical energy storage, Solar Energy 220 (2021) 432–439.

[29] N. Lin, C. Li, D. Zhang, et al., Emerging phase change cold storage materials derived from sodium sulfate decahydrate, Energy 245 (2022) 123294.

[30] Z. Kazemi, S.M. Mortazavi, A new method of application of hydrated salts on textiles to achieve thermoregulating properties, Thermochimica Acta 589 (2014) 56–62.

[31] Y. Liu, Y. Yang, Preparation and thermal properties of $Na_2CO_3 \cdot 10H_2O$-$Na_2HPO_4 \cdot 12H_2O$ eutectic hydrate salt as a novel phase change material for energy storage, Applied Thermal Engineering 112 (2017) 606–609.

[32] Y. Liu, Y. Yang, Form-stable phase change material based on Na2CO3·10H2O-Na2HPO4·12H2O eutectic hydrated salt/expanded graphite oxide composite: The influence of chemical structures of expanded graphite oxide, Renewable Energy 115 (2018) 734–740.

[33] Y. Liu, Y. Yang, Use of nano-α-Al_2O_3 to improve binary eutectic hydrated salt as phase change material, Solar Energy Materials and Solar Cells 160 (2017) 18–25.

[34] X. Man, H. Lu, Q. Xu, et al., Review on the thermal property enhancement of inorganic salt hydrate phase change materials, Journal of Energy Storage 72 (2023) 108699.

[35] P. Royo, V.J. Ferreira, A.M. López-Sabirón, et al., Hybrid diagnosis to characterise the energy and environmental enhancement of photovoltaic modules using smart materials, Energy 101 (2016) 174–189.

[36] Z. Zhu, Y. Liu, Z. Zhang, et al., Studying carbon fiber composite phase change materials: Preparation method, thermal storage analysis and application of battery thermal management, Journal of Energy Storage 67 (2023) 107586.

[37] P. Ping, X. Dai, D. Kong, et al., Experimental study on nano-encapsulated inorganic phase change material for lithium-ion battery thermal management and thermal runaway suppression, Chemical Engineering Journal 463 (2023) 142401.

[38] Z. Ling, S. Li, C. Cai, et al., Battery thermal management based on multiscale encapsulated inorganic phase change material of high stability, Applied Thermal Engineering 193 (2021) 117002.

[39] J. Li, J. Huang, Z. Liu, et al., Developing ternary composite phase change materials with two different phase change temperatures for battery thermal management, Applied Thermal Engineering 227 (2023) 120357.

Declaration of interests

☒ The authors declare that they have no known competing financial interests or personal relationships that could have appeared to influence the work reported in this paper.

☐The authors declare the following financial interests/personal relationships which may be considered as potential competing interests: